Effect of loading configuration and edge defect on the biaxial flexural behavior of annealed and chemically strengthened aluminosilicate glass plates

Zhen Wang, Letong Zhang, Yanpeng Gong

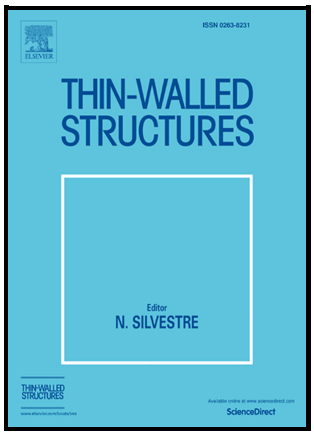

PII: S0263-8231(26)00451-9

DOI: https://doi.org/10.1016/j.tws.2026.114927

Reference: TWST114927

To appear in: *Thin Walled Structures*

Received date: 13 June 2025
Revised date: 31 December 2025
Accepted date: 1 April 2026

Please cite this article as: Zhen Wang, Letong Zhang and Yanpeng Gong, Effect of loading configuration and edge defect on the biaxial flexural behavior of annealed and chemically strengthened aluminosilicate glass plates, *Thin Walled Structures,* (2026) doi:https://doi.org/10.1016/j.tws.2026.114927

Effect of loading configuration and edge defect on the biaxial flexural behavior of annealed and chemically strengthened aluminosilicate glass plates

Zhen Wang, Letong Zhang, Yanpeng Gong*

Department of Mechanics, Beijing University of Technology, Beijing 100124, PR China

*Corresponding author: Yanpeng Gong (yanpeng.gong@bjut.edu.cn)

Abstract: Glass plates are widely used as load-bearing components in engineering structures. If the design of the glass frame is unreasonable or there are defects at the edges of the glass panels, fracture can be triggered accidently from the edge of glass panels under biaxial flexural loading conditions. In this study, two loading configurations of biaxial flexural tests, including Ball-On-Ring (BOR) and Ring-On-Ring (ROR), have been conducted on both annealed glass (AG) and chemical strengthened glass (CSG) plates. Three-dimensional Digital Image Correlation (3D-DIC) technique was utilized with specially designed loading fixture to obtain the real-time deformation field of glass plates. Edge defects were fabricated on the specimens to further evaluate the influence on biaxial flexural strength and failure mode. Numerical analysis was performed to extract the stress distribution of glass panels under different biaxial flexural loading configurations. The effect of edge defect depth and width on stress concentration has been illustrated. The influence of chemically residual stress on the biaxial flexural behavior of aluminosilicate glass plates was also clarified, thereby providing technical support for the reliability analysis of engineering thin-walled glass components.

Keywords: Aluminosilicate glass; biaxial flexural loading; edge defect; residual stress.

Nomenclature

σ_{BOR}	Biaxial flexural strength based on BOR tests
σ_{ROR}	Biaxial flexural strength based on ROR tests
P	Peak load
R	Radius of specimen
R_S	Radius of support ring
R_L	Radius of loading ring
h	Thickness of specimen
r	Radius of loading ball
b	Equivalent radius of contact area
z	Actual radius of contact area
E'	Equivalent Young's modulus
μ	Poisson's ratio
3PB	Three-point-bending
4PB	Four-point-bending
AG	Annealed glass
CSG	Chemical strengthened glass
BOR	Ball-On-Ring
ROR	Ring-On-Ring
3D-DIC	Three-dimensional Digital Image Correlation
SEM	Scanning electron microscope
EDS	Energy dispersive spectrometer
SD	Standard deviation
CV	Coefficient of variation

1. Introduction

Silicate glass has diverse industrial applications as structural and functional integration structures due to its transparency, mechanical properties and chemical stability. It's used not only for building facades, aircraft windshields and bullet proof

systems, but also for display windows and glass substrates of electronic devices. Silicate glass is a typical brittle material possessing high compression strength but low tension/flexural strength[1,2]. Its mechanical response is liner elastic with quite small fracture strain. Flexure induced suddenly tensile failure remains a challenging issue for glass engineering structures[3,4].

Much efforts have been spent to strengthen glass products, such as fire-polishing, etching, thermal tempering and chemical strengthening[5]. Chemical strengthened glass (CSG) products are widely used in electronic devices, pharmaceutical containers and aircraft windshields[6–8]. Ion-exchange, also known as chemical strengthening, is an efficient technique to improve the mechanical strength of glass materials with no measurable optical distortion[9]. After ion-exchange process, strong compression stress at the surface of glass plates can be built to suppress the nucleation and propagation of surface microcracks. The ion-exchange layer depth is in the range of tens to hundreds of microns, which is comparable to the surface microcracks. Thus, the flexural strength of CSG is not simply the sum of annealed glass (AG) strength and surface compression stress[10–13]. It's essential to conduct quantitative analysis on the flexural strength of CSG under different loading conditions.

Three-point-bending (3PB) and Four-point-bending (4PB) tests are common testing methods for flexural strength evaluation of glass plates[14,15]. However, the measured flexural strength data is highly affected by the edge or conner defects of plate shaped glass specimens[16,17]. The obtained flexural strength is actually uniaxial flexural behavior while the tensile side of the specimen is under uniaxial tension during loading process. For some realistic applications, such as aircraft windshield under pressure loading or bird impact, the glass structure is under biaxial flexural loadings[18,19]. Thus, it's essential to evaluate the biaxial flexural behavior of AG and CSG[20,21]. Two equi-biaxial flexural loading methods, Ball-On-Ring (BOR) and Ring-On-Ring (ROR), have been utilized in this study to evaluate the biaxial flexural mechanical behavior of glass structures.

The flexural strength of silicate glass depends primarily on initial microcracks during manufacturing and defects during usage[22–25]. The crack system during cutting

process has been investigated and the cutting process parameters will affect the mechanical quality of processed glass edges[26,27]. Small defects, such as scratches, have obvious influence on the flexural performance of glass specimens. Scratched glass panels show a significant decrease in flexural strength for both annealed and strengthened specimens[28–30]. For BOR and ROR loading conditions, the center region of the glass plate is under uniform equi-biaxial tension, leading to biaxial tensile fractures at the center region of the specimens. Introducing defects in the central area can offer a straight forward way to study the effects of defects on biaxial flexural strength. The residual flexural performance of scratched glass depends on the characteristics of the scratch location, distribution and scratch morphology[31,32]. The research content of the present study is derived from engineering practice. In the design of aircraft windshields and bird impact tests conducted by the authors, the glass plates are subjected to typical biaxial bending loading conditions. If the design of the glass frame is unreasonable or there are defects at the edges of the glass, fractures may occur at the edges of the glass plates. Another typical case is the glass curtain wall subjected to hurricane loads. The stress at the glass edges depends on the mechanical support conditions. The loading condition, such as the loading area on the plates, and also the geometry of glass plates can also influence the magnitude of edge stresses. Generally, the edge stress of a loaded glass plate is lower than the stress at the center. However, in the presence of edge defects, stress concentration may occur at the tip of the defects, potentially resulting in locally elevated stress levels. Thus, the edge defects can cause cracks initiation from the edges. However, research on the effect of edge defects for specimens under biaxial flexural loading is still limited. Conducting stress analysis on the edge of glass plates under biaxial flexural loadings is essential for strength assessment of glass components and failure analysis of glass structures with all edges simply supported.

The purpose of this study is to illustrate the effect of edge defects and chemical strengthening residual stress on the biaxial flexural behavior of aluminosilicate glass plates. Two loading configurations of biaxial flexural tests including BOR and ROR have been conducted on AG and CSG plates, providing a comprehensive performance

assessment of aluminosilicate glass. Edge defects were fabricated on the specimens to further evaluate the influence on biaxial flexural strength. The biaxial flexural failure modes of glass specimens were compared in detail. Further numerical and theoretical analysis revealed the effects of different loading forms, edge defects and chemical strengthening residual stress on biaxial flexural behavior of glass plates. This study can contribute to the biaxial flexural strength assessment of glass components and fracture analysis of glass structures.

2. Glass specimens and biaxial flexural tests

2.1 Specimens preparation

The material used in this study is aluminosilicate glass with a higher content of alumina compared to soda-lime glass. Aluminosilicate glass is suitable for Na^+ and K^+ ion-exchange and strengthened glass is widely used in load bearing components such as aircraft windshields and cell phone screens[33,34]. The FSM-6000LE surface stress meter was used to measure the surface stress of CSG and the compression stress is around 600 MPa. The FEI Verios G4 scanning electron microscope (SEM) with energy dispersive spectrometer (EDS) was utilized to detect the content of Na^+ and K^+ along the thickness direction of the glass plates. Fifteen points along the thickness direction of the glass specimen were selected on the fracture surface for detection, as shown in Fig. 1 (a). The weight percentage of Na^+ at point 1 is the lowest while the weight percentage of K^+ at point 1 is the highest. When the depth of the detection point exceeds 10 μm, the ion weight percentage tends to stabilize. Thus, the ion-exchange layer depth is around 10 μm for CSG. Gradient compressive residual stress can be found at the surface layer of CSG. Accordingly, a balancing small tensile stress will be formed at the inner of the glass plates. The diameter of the glass plates is 122 mm and the thickness is 6 mm. To study the effect of edge defects, some specimens were fabricated with a notch at the edge via STX-202A diamond line saw cutting machine, as shown in Fig. 1 (b). The fabricated depth and width of the notch are 1.0 mm and 0.4 mm respectively. The width 0.4 mm is based on the diameter of diamond line saw. The depth of 1 mm is just selected as a typical value for analysis and detailed parametric studies

have also been conducted in section 5.

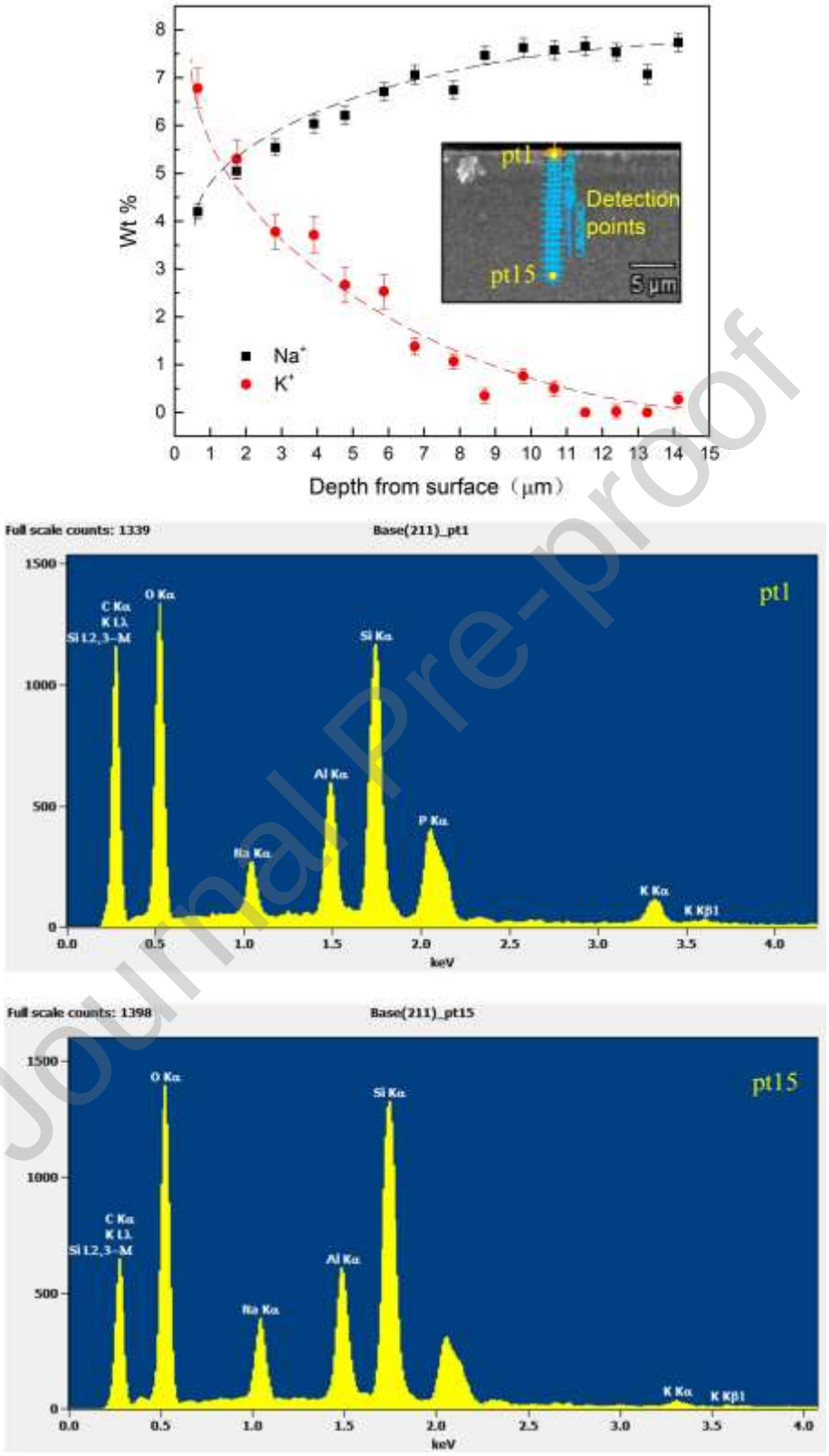

(a) Characterization of CSG compression layer thickness by detecting the weight percentage of Na^+ and K^+ based on SEM-EDS device.

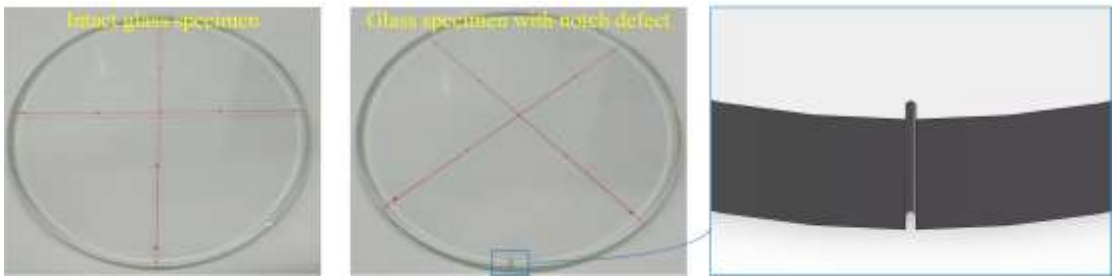

(b) Intact and notched glass plate specimens used in present study. The diameter of the glass plates is 122 mm and the thickness is 6 mm.

Fig. 1. Material characterization and specimen preparation

2.2 BOR and ROR tests

During biaxial flexural tests, the plate specimens were placed on the support ring with a diameter of 110 mm. The specimens were then loaded by a steel ball or a smaller circular ring, corresponding to BOR and ROR tests illustrated in Fig. 2 (a) and (b). All test fixtures are made of high-strength martensitic alloy steel after heat treatment. The test fixture directly loads the samples without interlayers. The tensile surfaces of disc specimens within the loading ball contact area (for BOR tests) or loading ring area (for ROR tests) undergo biaxial tension during tests[35].

During BOR tests, the equi-biaxial flexural strength σ_{BOR} can be calculated by[36]:

$$\sigma_{BOR} = \frac{3P(1+\mu)}{4\pi h^2}\left[1 + 2ln\left(\frac{R_s}{b}\right) + \frac{1-\mu}{1+\mu}\left(1 - \frac{b^2}{2{R_s}^2}\right)\frac{{R_s}^2}{R^2}\right] \quad (1)$$

where P is the applied peak load and μ is the Poisson's ratio. R, R_S and h represent the radius of specimen, radius of support ring, thickness of specimen respectively, as shown in Fig. 2 (a). The equivalent radius b of the contact area between the ball and specimen can be calculated as followed. z represents the actual contact radius of the contact area obtained based on the Hertz elastic contact theory[37]. r is the radius of loading ball and E' is the equivalent Young's modulus.

$$b = \begin{cases} z, & for\ z > 1.724h \\ (1.6z^2 + h^2)^{1/2} - 0.675h, & for\ z < 1.724h \\ 0.325h, & for\ z \to 0 \end{cases} \quad (2)$$

$$z = \left(3Pr/4E'\right)^{\frac{1}{3}} \quad (3)$$

$$E^{'-1} = \frac{1-\mu_1{}^2}{E_1} + \frac{1-\mu_2{}^2}{E_2} \quad (4)$$

where the subscribes 1 and 2 represent the loading ball and glass specimen respectively. Thus, μ_1=0.3, μ_2=0.22, E_1=200 GPa, E_2=75 GPa, r=8 mm. z can be calculated as 0.624 mm, which is smaller than 1.724h. In this condition, b can be defined by equation (2) as 2.002 mm.

The ROR equi-biaxial flexural strength σ_{ROR} can be calculated via plate bending theory[38,39]:

$$\sigma_{ROR} = \frac{3P}{2\pi h^2}\left[(1-\mu)\frac{R_S{}^2 - R_L{}^2}{2R^2} + (1+\mu)ln\frac{R_S}{R_L}\right] \quad (5)$$

where R_L represent the radius of the loading ring, as shown in Fig. 2 (b). Thus, R_S is 55 mm for both BOR and ROR tests and R_L=25 mm, R=61 mm, h=6 mm. In the following text, BOR/ROR strength refers to the BOR/ROR equi-biaxial flexural strength.

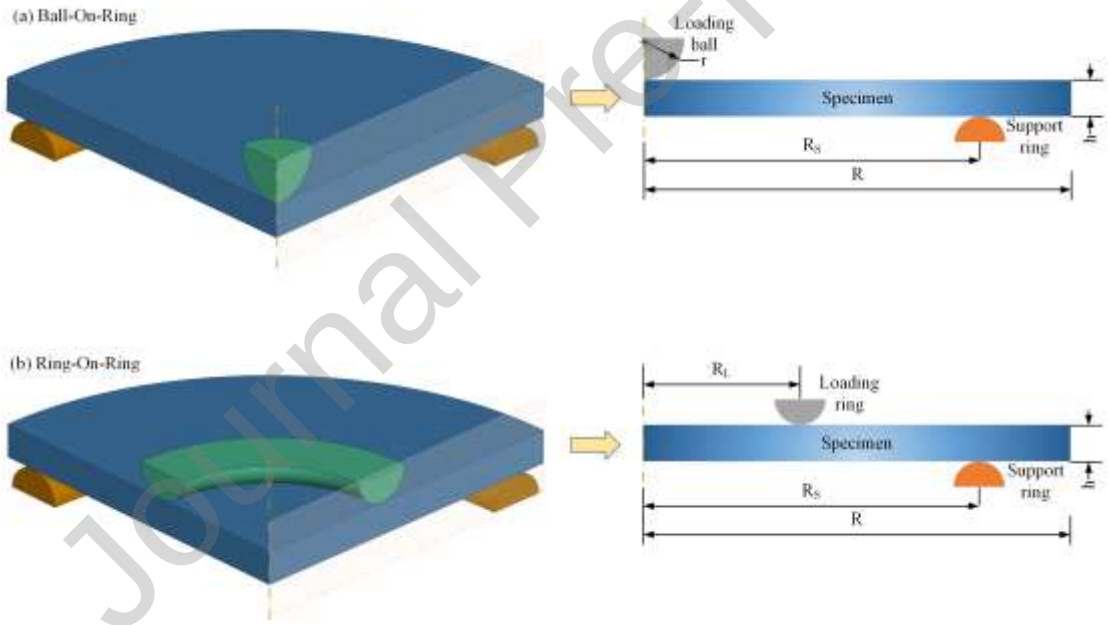

Fig. 2. Loading configurations of BOR and ROR biaxial flexural tests.

2.3 Experimental setup

The glass disc specimens were loaded by a universal testing machine at a quasi-static loading velocity of 0.2 mm/min. The corresponding stress rates for BOR and ROR loadings are 1.36 MPa/s and 0.73 MPa/s respectively, which is close to the suggested stress rate 2 MPa/s in accordance with the European standard EN 1288-2/-5[40,41]. The stress rate significantly influences material strength only when there is a change of

one order of magnitude or greater[42]. Thus, the BOR and ROR strength data in this study is reasonable and comparable. To monitor the out-of-plane displacement and in-plane strain of the tensile surface of specimens, a specially designed loading fixture was used with 3D-DIC technique[43]. A flat and front-silvered mirror was placed below the glass plate exactly at 45-degree orientation. Thus, the two cameras can monitor the deformation of glass plate from different directions. A pair of synchronized images were then recorded with the time intervals of 1 second by these two cameras. The experimental setup is shown in Fig. 3.

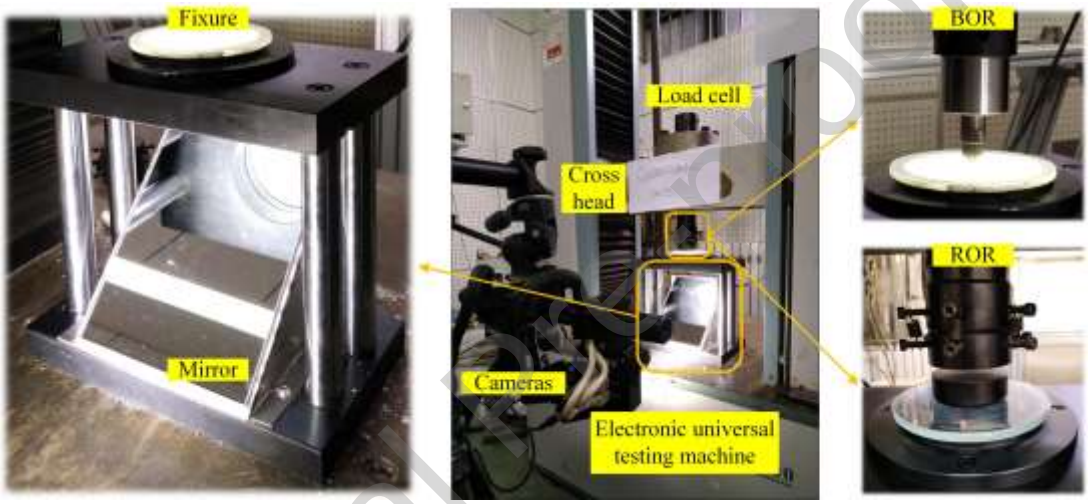

Fig. 3. Experimental setups for biaxial flexural tests with 3D-DIC technique.

3. Experimental results and analysis

3.1 Biaxial flexural strength

Glass plates with and without edge defects were loaded via both BOR and ROR biaxial flexural tests. The purpose of the experimental tests is to characterize the load-bearing capacity of the glass plate structure with and without edge defect under different loading conditions. For convenience of comparison, the equi-biaxial flexural stress value at which the glass plate loses its load-bearing capacity is recognized as its equi-biaxial flexural strength regardless of the failure origin. Three repeated tests were conducted under each loading condition, which cannot be used for statistics analysis but sufficient for illustrating general correlations. All the experimental data, including average biaxial flexural strength, standard deviation (SD) and coefficient of variation (CV), are provided in Table 1 and also plotted in Fig. 4 for comparison. It can be seen

that the obtained average biaxial flexural strength values are different for different loading configurations. The BOR biaxial flexural strengths of intact AG and CSG specimens are 91.2% and 59.2% higher than their ROR biaxial flexural strengths. For comparison of specimens with and without edge defects, there is nearly no difference for AG specimens under BOR loading condition. However, the average BOR biaxial flexural strength of CSG specimens with edge defects is 431.1 MPa, 40.4% lower than that of intact specimens. Under ROR loading condition, the biaxial flexural strength decreases by 48.3% and 65.1% for AG and CSG specimens when existing edge defects.

Table 1 Equi-biaxial flexural strength data (MPa)

Loading type	Number of specimens	AG-intact	AG-edge defect	CSG-intact	CSG-edge defect
BOR biaxial flexure	No. 1	155.1	163.7	743.6	444.9
	No. 2	152.6	152.9	679.5	432.3
	No. 3	149.5	143.9	746.1	416.1
	Ave.	152.4	153.5	723.1	431.1
	SD	2.8	9.9	37.7	14.4
	CV	0.02	0.06	0.05	0.03
ROR biaxial flexure	No. 1	92.7	44.7	468.7	139.3
	No. 2	76.3	38.7	389.4	151.9
	No. 3	70.1	40.3	504.5	184.5
	Ave.	79.7	41.2	454.2	158.6
	SD	11.7	3.1	58.9	23.3
	CV	0.15	0.08	0.13	0.15

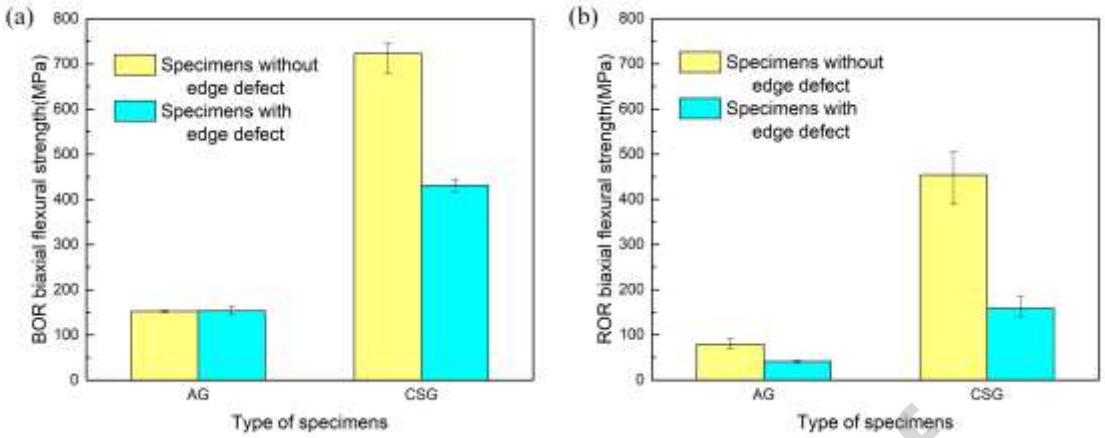

Fig. 4. Equi-biaxial flexural strength of AG and CSG obtained from (a) BOR and (b) ROR loading conditions. The height of the bars represents the average biaxial flexural strength, and the range of the error bars represents the biaxial flexural strength range obtained from the experiments.

3.2 Deformation field

The full-field out-of-plane displacement nephogram can be obtained from 3D-DIC technique, as shown in Fig. 5. Representative results for both BOR and ROR loading conditions of AG and CSG specimens are shown in Fig. 5 (a) (b) (c) (d) respectively. The letters A, B, C, D, E, F marked in the figure represent different moments during the loading process. The letter A represents the moment upon loading and the letter F is the moment upon fracture of the glass plates. These results confirm the effectiveness of the biaxial tests aided by 3D-DIC technique, enabling the comparison of the deformation capabilities of AG and CSG under different equi-biaxial loading conditions, and can also be used for subsequent comparison and validation of numerical models. It should be noted that the edge defect has no influence on the deformation distribution and thus only intact specimens are analyzed in this section. It can be seen that the out-of-plane displacement of CSG is much higher than AG under both loading conditions. For the same type of glass, the specimens get a higher out-of-plane displacement under ROR loading compared to BOR.

The out-of-plane displacement data along the diameter of glass plates are extracted and plotted in Fig. 6 (a) (b) (c) (d), corresponding to the time moments shown in Fig. 5. It can be seen that the center points of the disc specimens exhibit the maximum out-

of-plane displacement for all loading conditions. The displacement curve changes more gently at the center regions for ROR tests compared to BOR tests.

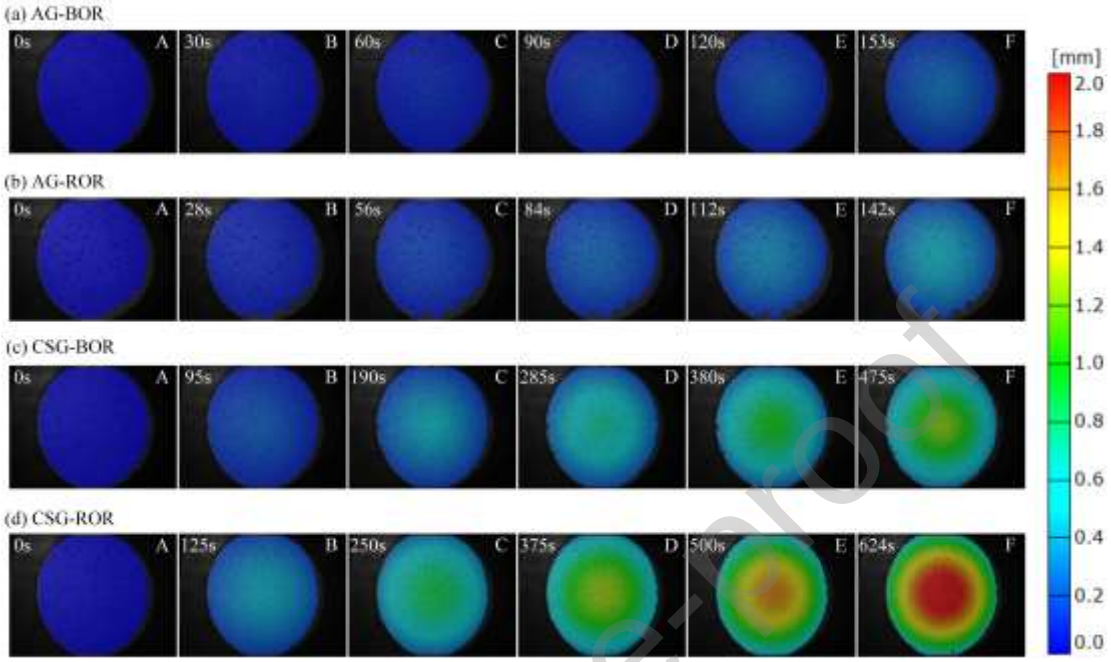

Fig. 5. Out-of-plane displacement of glass plates during biaxial flexural loading calculated using 3D-DIC.

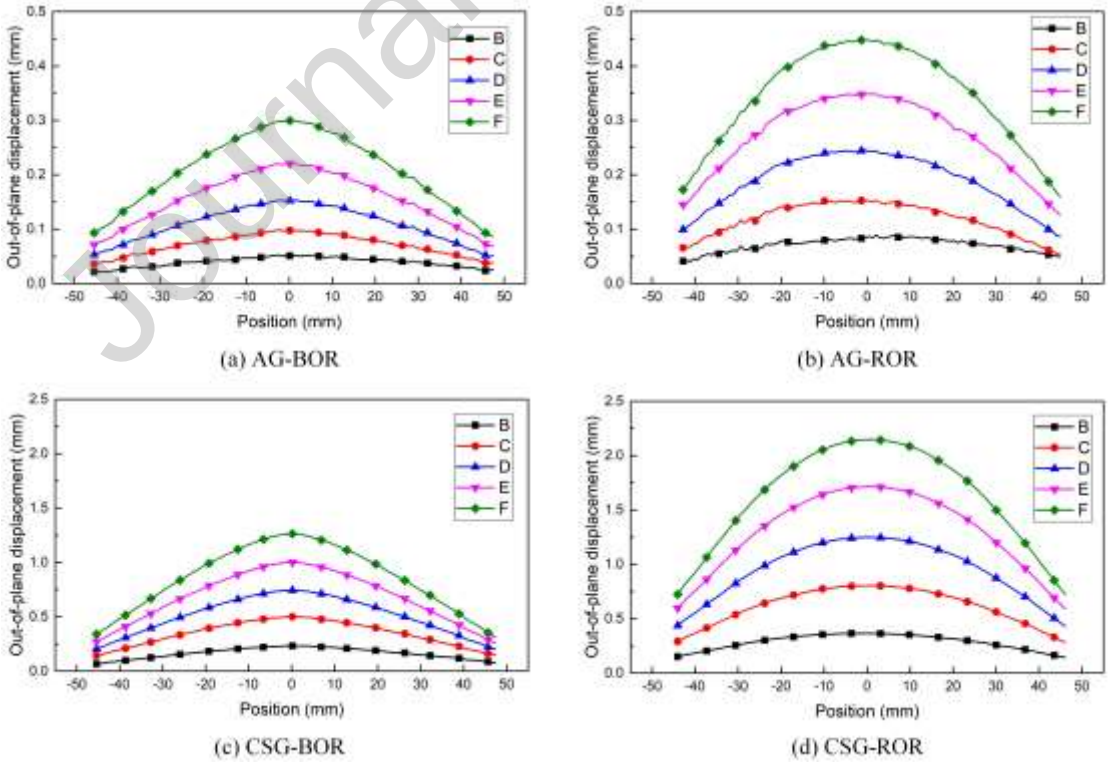

Fig. 6. History of out-of-plane displacement along the diameter of glass plates. (The capital letters

B-F correspond to the time moments shown in Fig. 5.)

The major principal strain history along the diameter of CSG plates under BOR and ROR loading is shown in Fig. 7 (a) and (b). Calculating strain from displacement is a differential process, which is sensitive to the accumulative errors. Thus, the strain curves are fluctuated compared to displacement curves. It can be seen that the major strain distribution on glass surface is totally different for BOR and ROR loading conditions. The BOR loading results in a gradient major strain distribution on the glass surface, with the peak value in the center of the specimen. In contrast, a uniform strain distribution field is formed below the load ring for the ROR specimens[35]. The maximum major strain for glass plates under BOR loading is higher than ROR, which exhibits different trend compared to the displacement results.

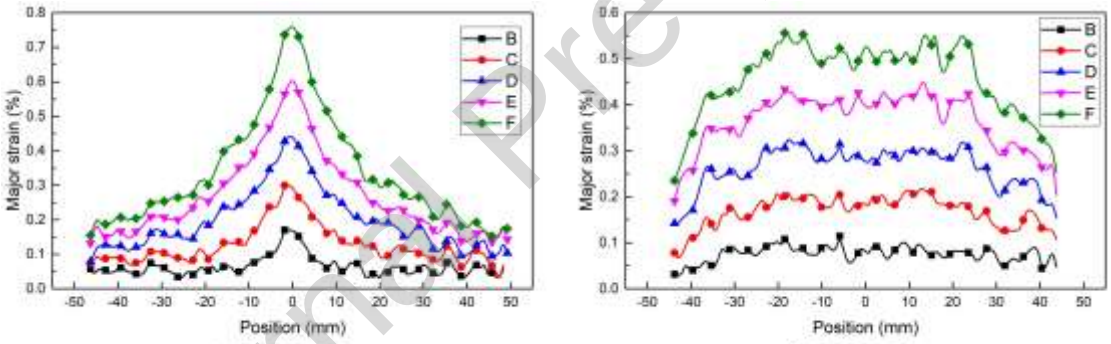

Fig. 7. History of major principal strain along the diameter of glass plates. (The capital letters B-F correspond to the time moments shown in Fig. 5.)

The out-of-plane displacement and major strain curves upon failure of the specimens are compared, as shown in Fig. 8 (a) and (b). The maximum out-of-plane displacements for AG under BOR and ROR loadings are 0.30 mm and 0.45 mm. While for CSG, they are 1.26 mm and 2.15 mm respectively. The maximum major strains for AG under BOR and ROR loadings are 0.18% and 0.11%. While for CSG, they are 0.76% and 0.52% respectively.

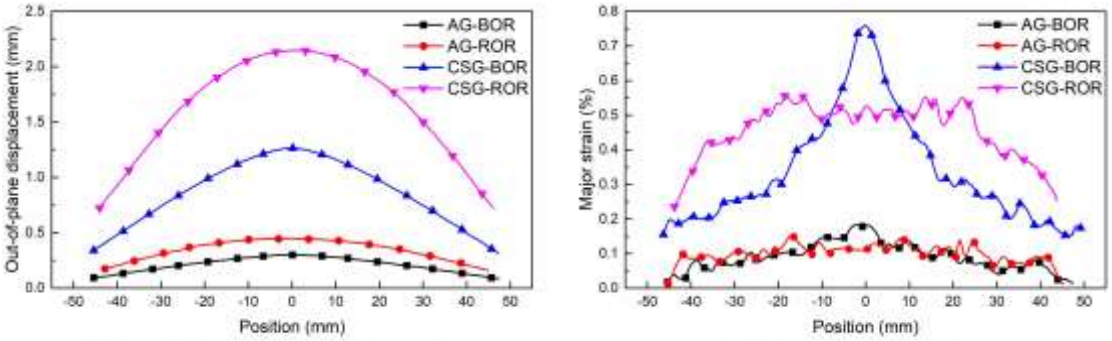

(a) Out-of plane displacement comparison (b) Major strain comparison

Fig. 8. Comparison of out-of-plane displacement and major principal strain of AG and CSG under BOR and ROR loading conditions.

3.3 Failure modes

Adhesive transparent tape was put on the top surface of the glass plates before tests to collect the fragments for failure modes analysis. As the transparent tape is very soft and thin at the compression surface, it won't affect the mechanical response of glass specimens. The general patterns of crack extension and branching not only point the way back to a fracture origin, but also provide information about the cause of fracture, the energy of fracture, and the stress state. The failure modes of glass plates under BOR flexural loadings are shown in Fig. 9. A gradient stress field is formed on the tensile surface of the specimen and the cracks start at the center and radiate outwards, as shown in Fig. 9 (a). The straight radial cracks distribute uniformly along the circumferential direction. The failure pattern shows no difference for AG with edge defects, as shown in Fig. 9(b). The crack origin is also at the loading point, in corresponding to the same BOR flexural strength of AG specimens with and without edge defects provided in Table 1. For intact CSG specimen, the fracture origin is also at the center shown in Fig. 9 (c). However, much more dense radial cracks appear and even with some lateral cracks, indicating a high strength failure type. The formation of multiple cracks is the process of releasing strain energy caused by both external loading and internal residual stress. More dense cracks locate around the center region because the center part undergoes a higher level of stress before fracture. For CSG specimens with edge defect shown in Fig. 9 (d), the fracture starts from the defect. The crack propagated and branched to multiple cracks when reaching the terminal velocity. The stress state of the

disc specimen changed with the development of cracks and thus the failure pattern is not regular radial crack pattern. The final failure mode is caused by the interaction of two crack systems.

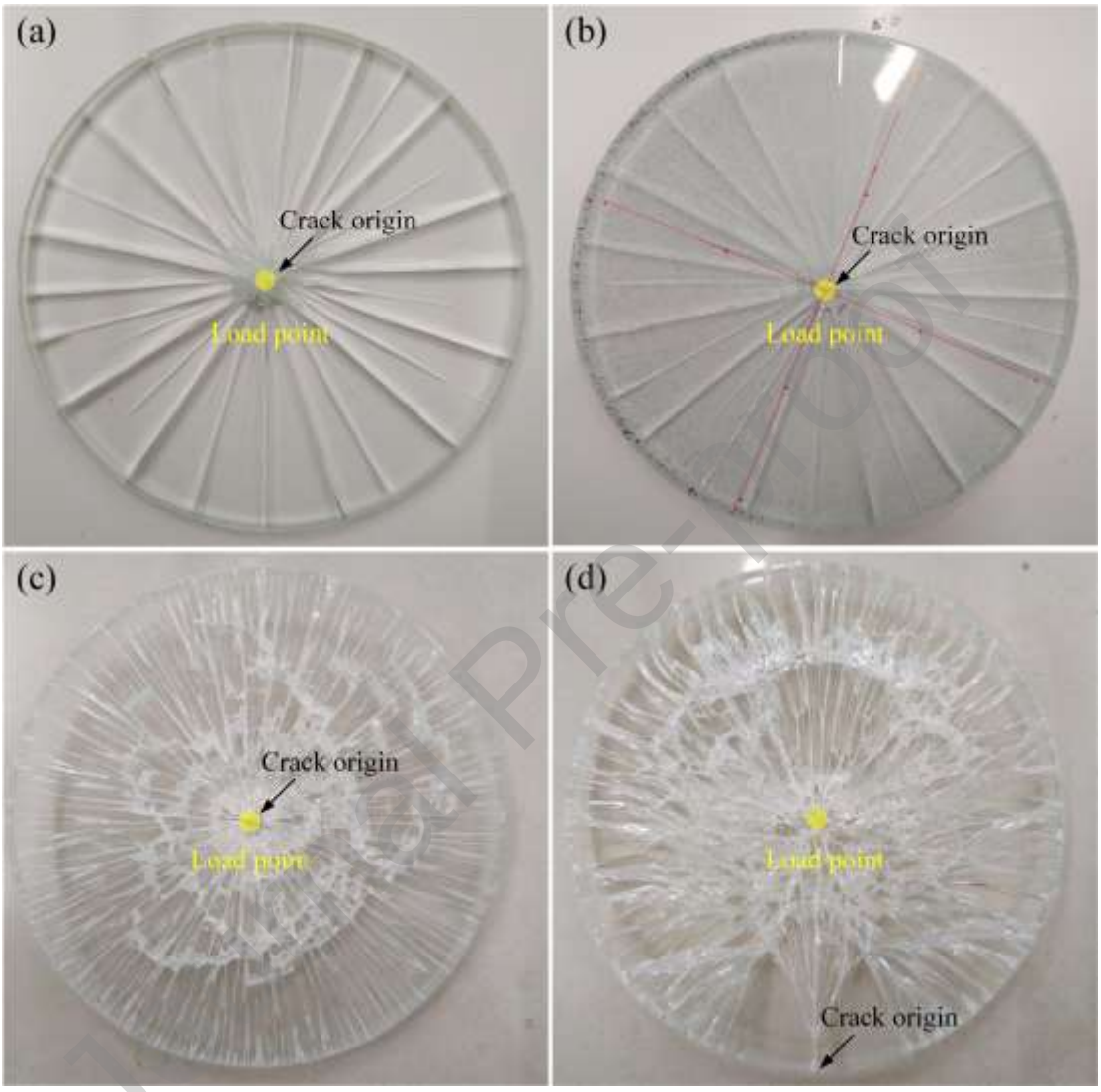

Fig. 9. Failure modes of glass plates under BOR flexural loadings: (a) AG-intact, (b) AG-edge defect, (c) CSG-intact, (d) CSG-defect.

For specimens under ROR loading, the failure modes are totally different. An equi-biaxially-stressed region is formed in the inner circle region without stress concentration. The crack origin for the AG specimen shown in Fig. 10 (a) is a pair of branches in opposite directions. Cross cracks appear at the inner ring area with radial cracks outside the inner ring. For AG with edge defect, the crack started from the defect, as shown in Fig. 10 (b). After the first break has occurred, the remnants still bear load

from the inner loading ring and break in bending. Less cracks formed in this specimen indicates a low strength condition, in corresponding to the loading data in Table 1. For intact CSG plate, the cracks are very dense and even the plate breaks into small particles at the inner ring region, as shown in Fig. 10 (c). For CSG specimen with edge defect shown in Fig. 10 (d), the fracture origin locates at the defect spot. Similar to BOR loading, the crack propagated and branched to multiple cracks when reaching the terminal velocity. Dense cracks formed along the specimen. However, two small regions around the initial crack are still transparent without cracks due to the rapid stress release at the initial crack propagation stage.

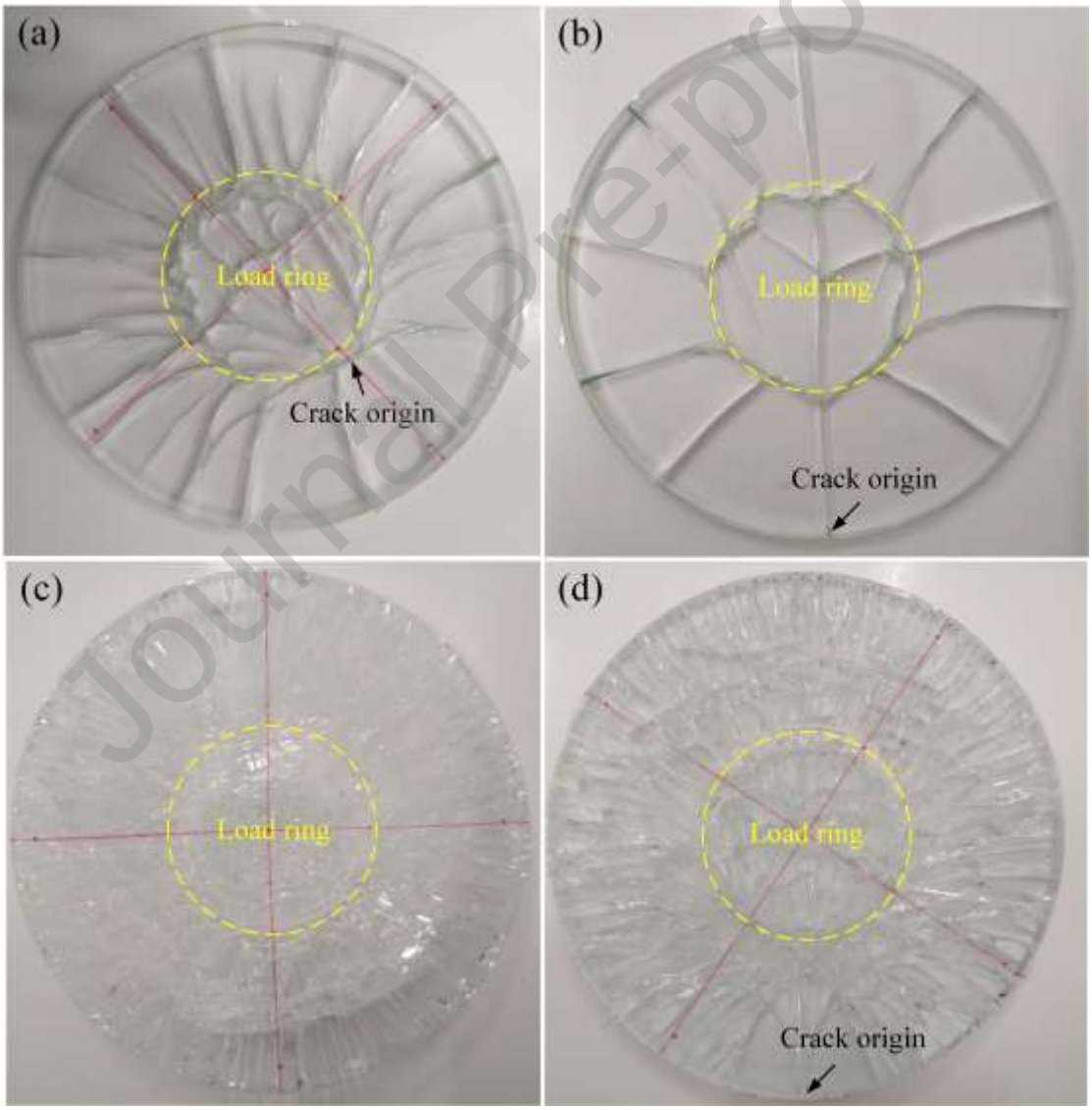

Fig. 10. Failure modes of glass plates under ROR flexural loadings: (a) AG-intact, (b) AG-edge defect, (c) CSG-intact, (d) CSG-defect.

4. Numerical models for stress analysis

To further illustrate the effect of loading forms, edge defects and chemical strengthening residual stress on the biaxial flexural response of glass plates, finite element analysis models were developed based on the commercial ABAQUS software. Eight-node linear hexahedral (C3D8R) elements were utilized for the numerical models. Both BOR and ROR tests are symmetrical loading configurations. Half models were utilized to reduce the calculation time, as shown in Fig. 11 (a) and (b). Contact interactions between the ring/ball fixture and glass plate are modeled using a surface-to-surface contact formulation. The tangential behavior is defined with a penalty friction coefficient of 0.2, and the normal behavior is set to "hard contact". The basic material parameters for steel fixture and aluminosilicate glass plates are shown in Table 2.

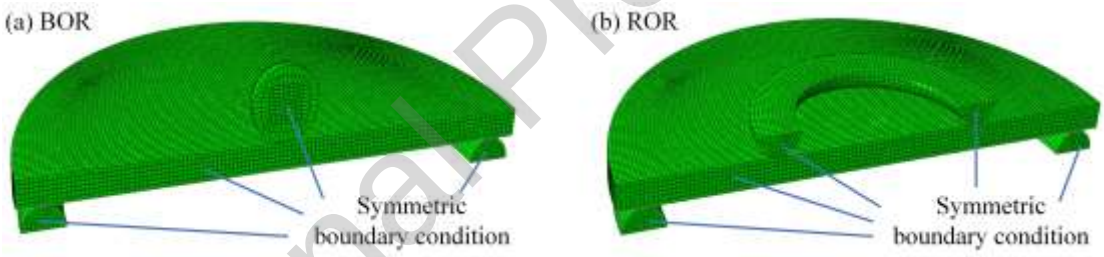

Fig. 11. Finite element models for BOR and ROR tests.

Table 2 Material parameters

Part	Density (kg/m^3)	Elastic Modulus (GPa)	Poisson's ratio
Loading fixture	7800	210	0.3
Glass plate	2546	75	0.22

4.1 Mesh size sensitivity analysis

Mesh size sensitivity analysis was then conducted. Different mesh sizes including 1.0 mm, 0.8 mm, 0.6 mm, 0.4 mm and 0.3 mm were used for building numerical models. The in-plane tensile stress of the center element at the tensile surface of the glass plate was extracted for comparison. The biaxial flexural stress – load relation was then

plotted and compared to the analytical solution based on equation (1) and equation (5). It can be seen from Fig. 12 (a) and (b) that with the decrease of mesh size, the numerical data become much closer to the analytical result. Also, the biaxial flexural stress – load relation is linear elastic for both loading conditions, indicating that the nonlinear effect can be neglected when the loading displacement is relatively low compared to the thickness of the glass sample[44,45].

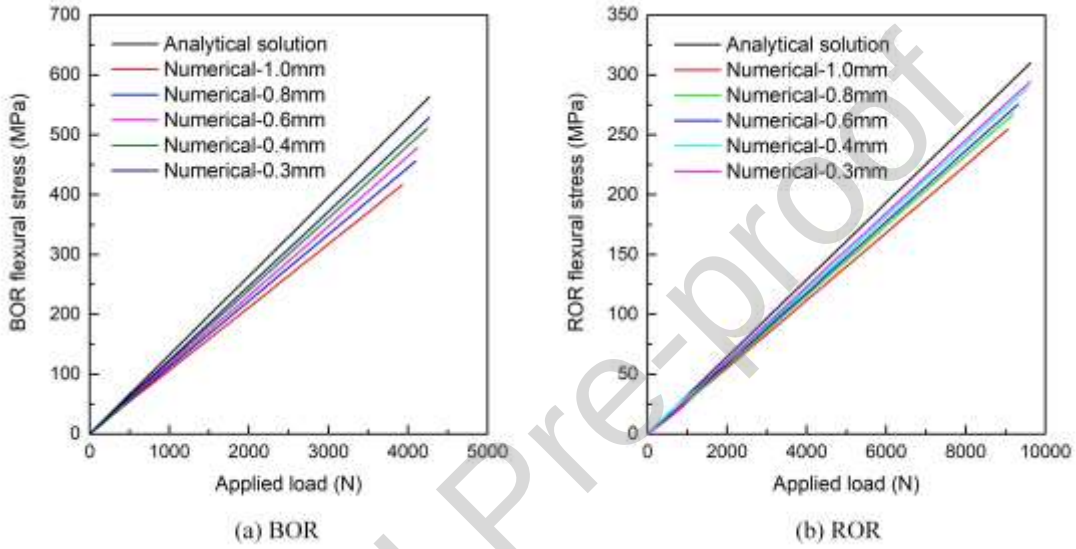

Fig. 12. Comparison between analytical solution of biaxial flexural stress and numerical results of different mesh sizes: (a) BOR, (b) ROR.

A detailed comparison for the BOR and ROR equi-biaxial flexural stress error between analytical solution and related numerical models as well as the calculation time are provided in Fig. 13 (a) and (b). For BOR loading condition, the error for numerical model with 1.0 mm mesh size is 18.3%, which decreases to 5.9% for the mesh size of 0.3 mm. For ROR loading condition, the error for numerical model with 1.0 mm mesh size is 13.6%, which decreases to 4.8% for the mesh size of 0.3 mm. For both loading conditions, the biaxial flexural stress represents the maximum biaxial tensile stress at the lower surface of the glass plate. For smaller mesh sizes, the surface elements can better mimic the surface tensile stress. This is the main reason for the mesh size sensitivity. For different mesh sizes of 1.0 mm, 0.8 mm, 0.6 mm, 0.4 mm and 0.3 mm, the calculation times for BOR models are 0.3 h, 0.7 h, 1.8 h, 7.3 h and 24.6 h

respectively by utilizing Intel(R) Xeon(R) Platinum 8168 CPU @ 2.70GHz with 24 cores. Similar computational efficiency was obtained for ROR models. To balance the computational efficiency and accuracy, the mesh size 0.4 mm was applied for both BOR and ROR models. The errors are 8.8% and 5.9%, which are fully acceptable for present study.

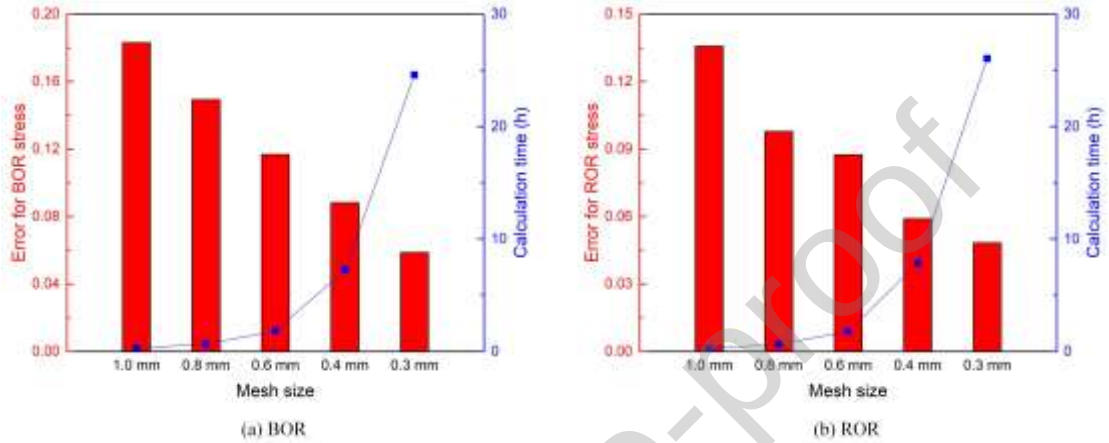

Fig. 13. Error between analytical solution and related numerical models as well as the calculation time comparison: (a) BOR, (b) ROR.

4.2 Numerical model validation

A comparison between experimental and numerical out-of-plane displacement data along the diameter of CSG plates under BOR and ROR loading at different loading stages was conducted, as shown in Fig. 14 (a) and (b). The major principal strain along the diameter of CSG plates under BOR and ROR loading is also compared in Fig. 15 (a) and (b). The calibrated mesh size 0.4 mm was applied for both BOR and ROR models. It can be seen that the numerical data can match the experimental curves very well.

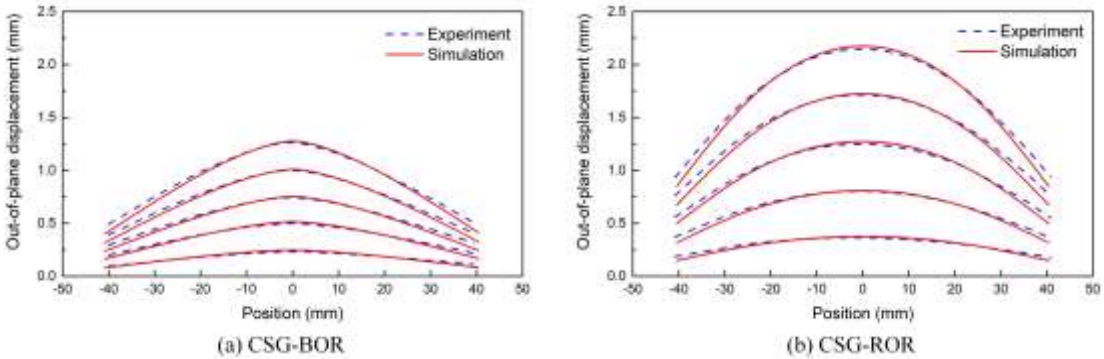

Fig. 14. Comparison of experimental and numerical out-of-plane displacement data along the diameter of glass plates at different loading stages.

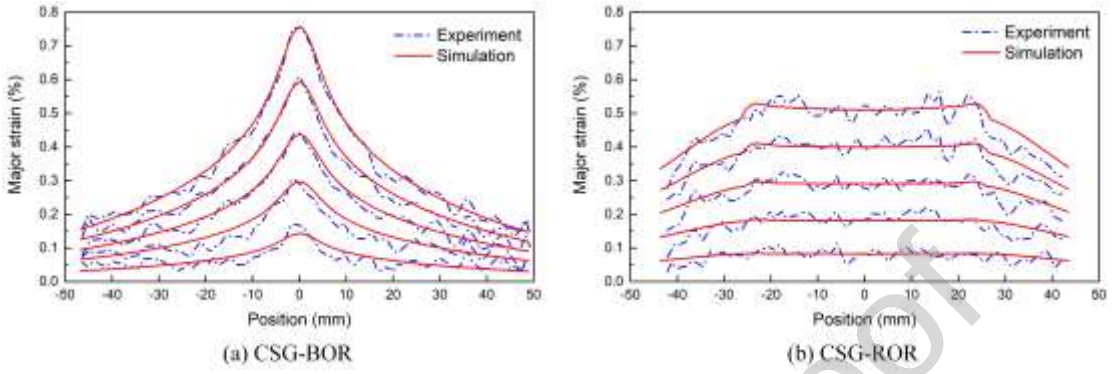

Fig. 15. Comparison of experimental and numerical major strain data along the diameter of glass plates at different loading stages.

5. Discussions

5.1 Effect of different loading forms

Although both BOR and ROR tests are standard testing methods for biaxial flexural strength evaluation of brittle materials, and the same specimens are utilized in these tests, different stress distributions can be seen in Fig. 16 (a) and (b) for different loading configurations. The radial and circumferential stress data along the diameter of the specimens are plotted following the cylindrical coordinate system. The same out-of-plane load 5000 N was applied for both BOR and ROR models. For BOR loading condition, the radial and circumference stress curves coincide at the center of the specimen, indicating an equi-biaxial flexural strength of 609.0 MPa. The radial stress decreased to zero while the circumference stress decreased to 68.4 MPa at the edge of the specimen. For ROR loading condition, the radial and circumference stress curves coincide at a much larger area below the loading ring, indicating a stable equi-biaxial flexural strength of 151.2 MPa. The radial stress decreased to zero while the circumference stress decreased to 56.1 MPa at the edge of the specimen. The small peaks at these curves for the position of ±55 mm are due to contact stress with support rings and won't affect the results. In conclusion, a much larger uniform biaxial stress region was formed under ROR loading and the BOR flexural stress is around 4 times

that of ROR flexural stress with the same loading force.

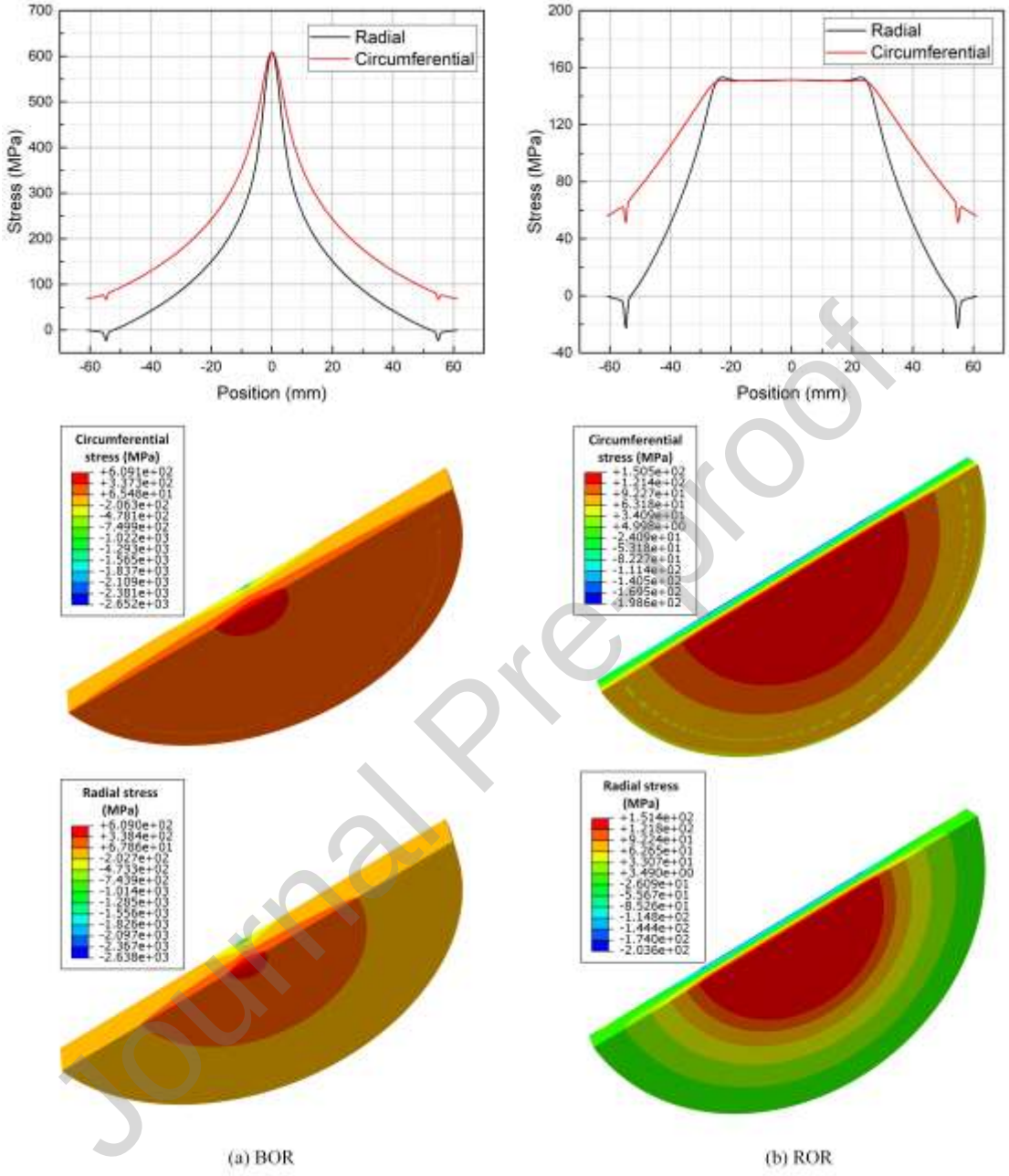

Fig. 16. Radial and circumferential stress distribution of the intact disc specimens under BOR and ROR loading conditions. The stress curves represent the stress distribution along the diameter of the specimen's lower surface.

There are a large number of randomly distributed micro-flaws on the surface of float glass generated from the producing process[22,46]. The flexural strength of glass is severely reduced compared to the theoretical strength due to stress concentrations

around these flaws[13,47]. During ROR loading condition, a large circular area is under uniform tension at the bottom surface of the specimen. Thus, more surface defects are under severe loading condition and tend to nucleate and propagate. However, during BOR loading, only a tiny area at the center of specimen is under maximum tension stress, as shown in Fig. 17. Due to the stochastic property of defects, the probability that the most severe defect is located in the maximum stress zone under BOR loading is much lower than under ROR loading. This is the primary cause for higher BOR strength compared to ROR strength for both AG and CSG shown in Table 1. It's reported that the uniaxial flexure strength of silicate glass shows size effect under three-point-bending tests[4]. The results in present study demonstrate "size effect" of aluminosilicate glass in biaxial flexural tests.

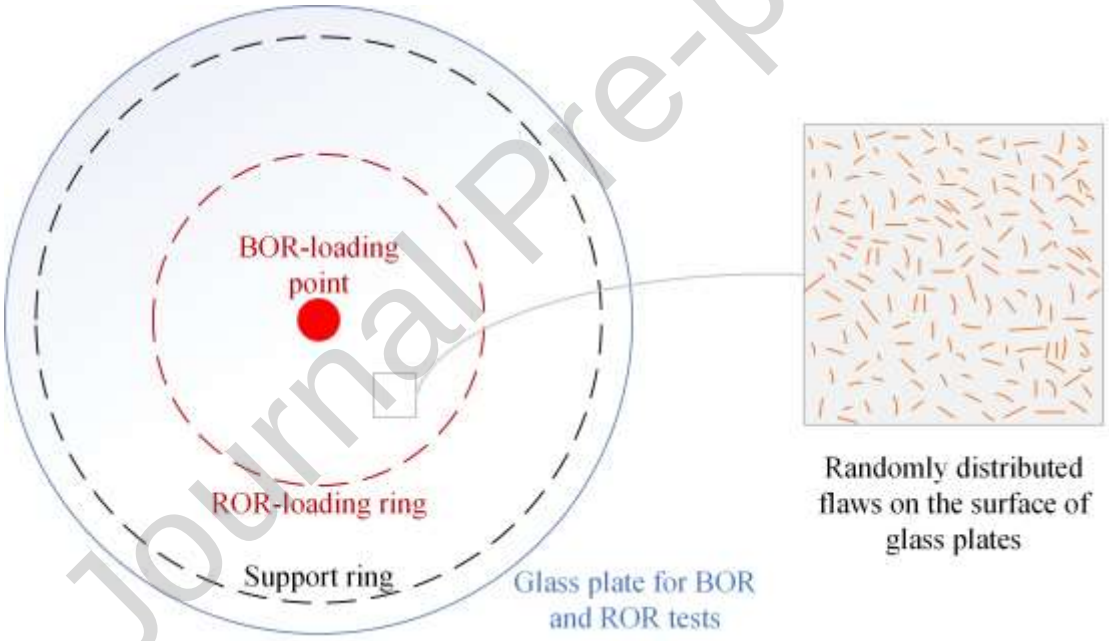

Fig. 17. Schematic diagram for the randomly distributed flaws on the surface of glass plates under BOR and ROR loadings.

5.2 Effect of chemical strengthening residual stress

Due to the existence of compression stress at the surface of aluminosilicate glass, the residual stress should be overcome first under tensile loading. Thus, the biaxial flexural strength of CSG is much higher than AG. According to the experimental results, the BOR flexural strength of CSG (723.1 MPa) is 570.7 MPa higher than AG (152.4 MPa),

while the ROR flexural strength of CSG (454.2 MPa) is 374.5 MPa higher than AG (79.7 MPa). Under both loading conditions, the differences of flexural strength between CSG and AG are lower than the residual compression stress of 600 MPa at the surface of CSG. This can be explained by the coupling effect of residual stress and microscopic surface flaws, as shown in Fig. 18. After the ion-exchange process, a surface compressive stress with a gradient distribution is formed on the surface together with a small internal tensile stress for balance. Due to the limitation of ion-exchange depth, the maximum compression layer depth is usually at several dozen micrometers[48,49]. The depth of surface flaws may be higher than compressive stress layer depth. A theoretical analysis based on the elastic fracture mechanics theory has been conducted and it's reported that the flexural strength of CSG cannot be simply evaluated by adding the residual compression stress to the flexural strength of AG[47]. The strengthening effect decreases with the increase of flaw depth.

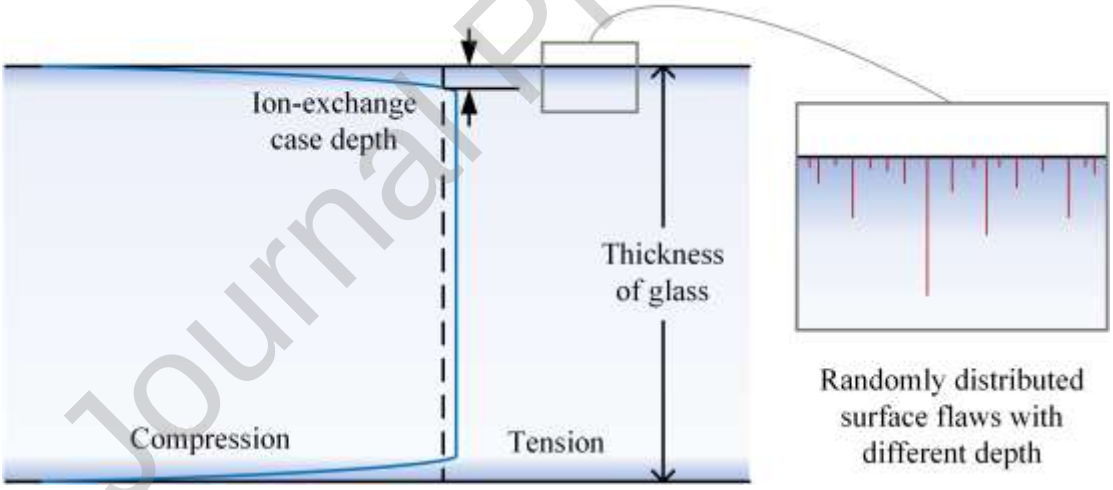

Fig. 18. Coupling effect of residual stress and microscopic surface flaws

On the other hand, the increased values of biaxial flexural strength due to chemical strengthening residual stress are different under BOR (570.7 MPa) and ROR (374.5 MPa) loading conditions. For BOR loading, the probability that deep cracks are located in the area with the maximum stress is very small. For ROR loading, there is a uniform circular tensile area at the bottom surface of glass specimen and deep flaws are likely to be exist in this area. As the strengthening effect decreases with the increase of flaw

depth, the strengthening effect has been better reflected during BOR loading condition.

5.3 Effect of edge defects

Numerical models were built to analyze the effect of edge defects on stress distribution of glass specimens under biaxial loading. The definitions of notch width, notch depth and notch tip radius are shown in Fig. 19 (a). The notch width is twice the value of notch tip radius. The glass specimen with notch is a symmetric structure as divided by the dot dash line. Thus, half models were utilized with symmetric boundary conditions for further analysis. The notch depth and width are 1 mm and 0.4 mm for the model shown in Fig. 19 (b) and (c). The meshes around the notch have been refined and validated.

Fig. 19. The definition of notch defect and related numerical models

For numerical specimens under BOR and ROR loading with notch depth 1 mm and notch width 0.4 mm, the same as the tested specimens with notch defect, the stress distribution nephogram and stress distribution curve along the axis of the specimen at the bottom surface are shown in Fig. 20 (a) and (b). The out-of-plane load 5000 N was applied for both BOR and ROR models, which is the same as the intact models. For

comparison with Fig. 16, the stress distribution at the central section of the specimens is nearly the same for intact and notched specimens. The difference of the biaxial stress at the center of the specimen is lower than 0.5% and thus can be neglected. This implies that a small notch defect won't affect the biaxial flexural strength testing results if the specimens break from the center region. However, the stress level at the notch tip is remarkably higher than the edge stress of intact specimens, especially for the circumferential stress. For the ROR loading condition, the edge stress is more sensitive to notch defect compared to BOR loading condition. The notch tip circumferential stress (169.0 MPa) of ROR specimen is even higher than equi-biaxial flexural stress (151.2 MPa). That means the glass specimens with this notch defect will tend to break from the notch instead of the center region under ROR loading condition at a lower biaxial stress level. This explains the experimental results on notched specimens provided in section 3. For intact and notched AG specimen, the BOR strength data is nearly the same and cracks initiate from the center point. However, the ROR strength of notched specimen is much lower with cracks initiating from the edge notch defect.

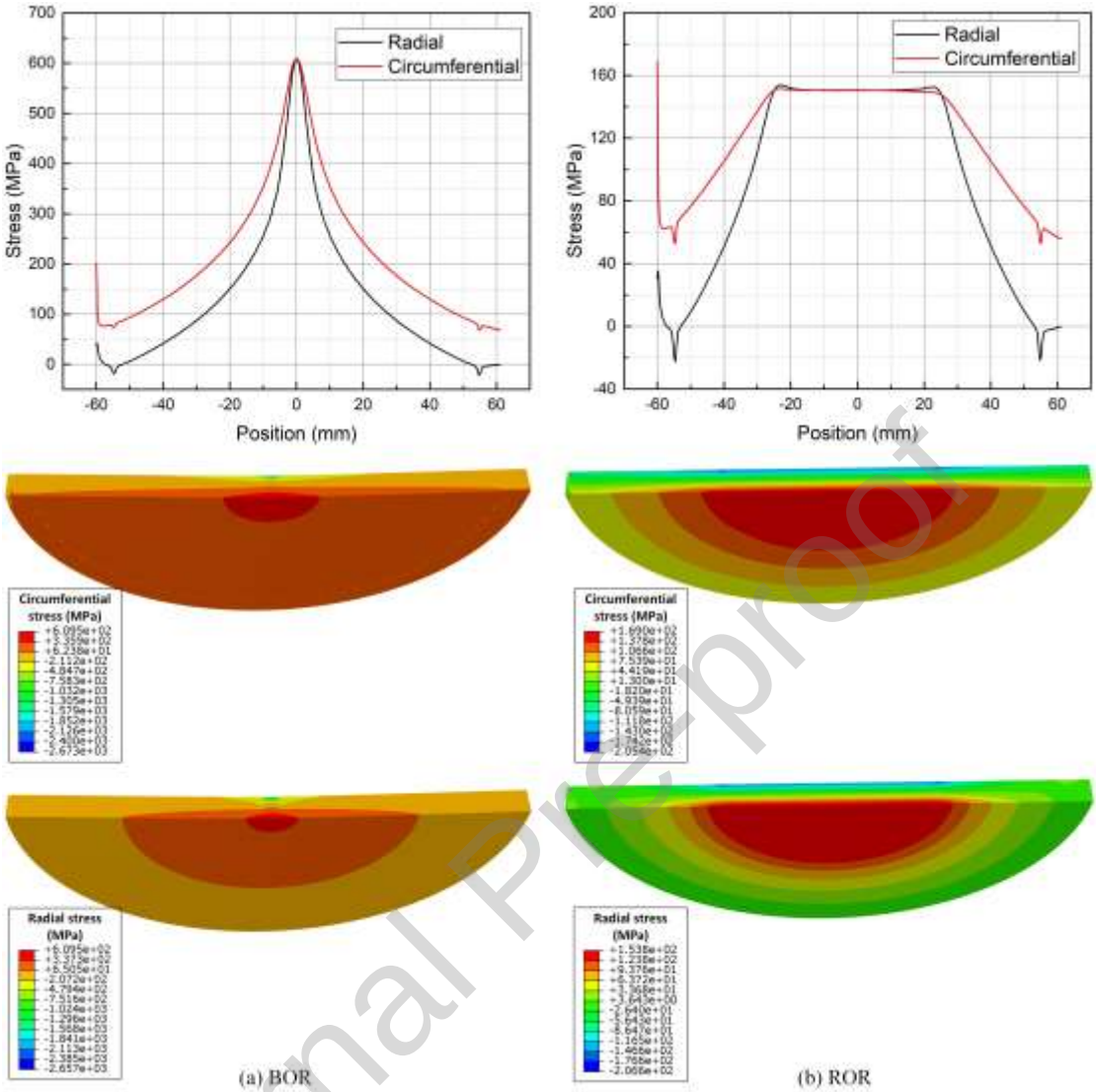

Fig. 20. Radial and circumferential stress distribution of the disc specimens with notch defects under BOR and ROR loading conditions. Stress concentration can be found at the notch region of the specimens.

The surface roughness with manufacturing defects has significant influence on the flexural strength of silicate glass[2,50,51]. It should be noted that rough surface formed during the manufacturing of notch defects by diamond line saw, which will further reduce the material strength around the notch[14]. Predicting the biaxial flexural strength of glass specimens with notch defects is still challenging. Quantitative stress analysis is conducted to illustrate the effect of notch shape. It can be seen from Fig. 16 that the circumferential stress at the edge of the disc specimen is much higher than radial stress. Thus, only the circumferential stress distribution will be considered in the

following parametric analysis. Fig. 21 (a) and (b) shows the effect of edge notch depth on circumferential stress distribution of glass specimens under BOR and ROR loading conditions. The edge notch width is fixed at 0.4 mm and the edge notch depth ranges from 0.2 mm to 2.0 mm. The curves of intact specimens are also plotted in the figure for reference. For both loading conditions, the edge stress increases with the increase of notch depth. Under BOR loading, the edge stress increases from 117.5 MPa to 263.4 MPa when the notch depth increases from 0.2 mm to 2.0 mm. Under ROR loading, the edge stress increases from 94.6 MPa to 227.8 MPa when the notch depth increases from 0.2 mm to 2.0 mm.

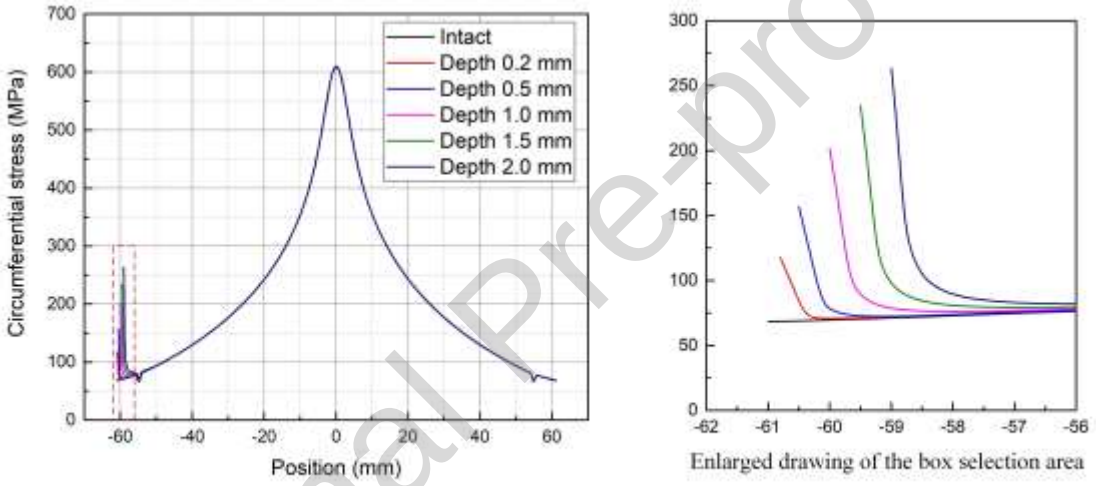

(a) BOR loading on specimens with edge notches of different depths

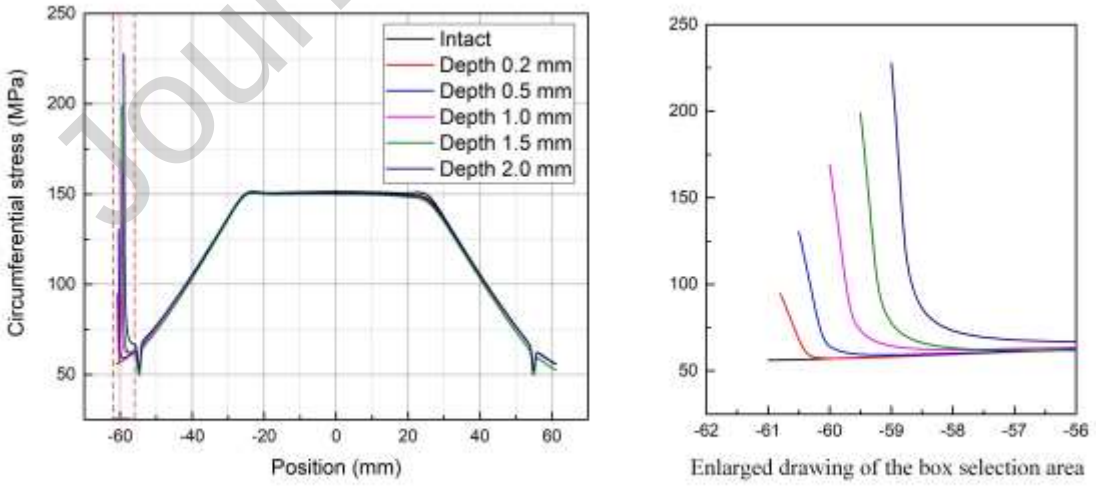

(b) ROR loading on specimens with edge notches of different depths

Fig. 21. Effect of edge notch depth on circumferential stress distribution of glass specimens under BOR and ROR loading conditions. The edge notch width is fixed at 0.4 mm.

Fig. 22 (a) and (b) shows the effect of edge notch width on circumferential stress distribution of glass specimens under BOR and ROR loading conditions. For this comparison, the edge notch depth is fixed at 1.0 mm. Numerical models with different notch widths of 0.3 mm, 0.4 mm, 0.6 mm, 0.8 mm and 1.0 mm were built. It can be seen that the stress concentration at the notch tip weakens with the increase of notch width. Under BOR loading, the edge stress decreases from 209.6 MPa to 167.0 MPa when the notch depth increases from 0.3 mm to 1.0 mm. Under ROR loading, the edge stress increases from 177.8 MPa to 139.8 MPa when the notch depth increases from 0.3 mm to 1.0 mm.

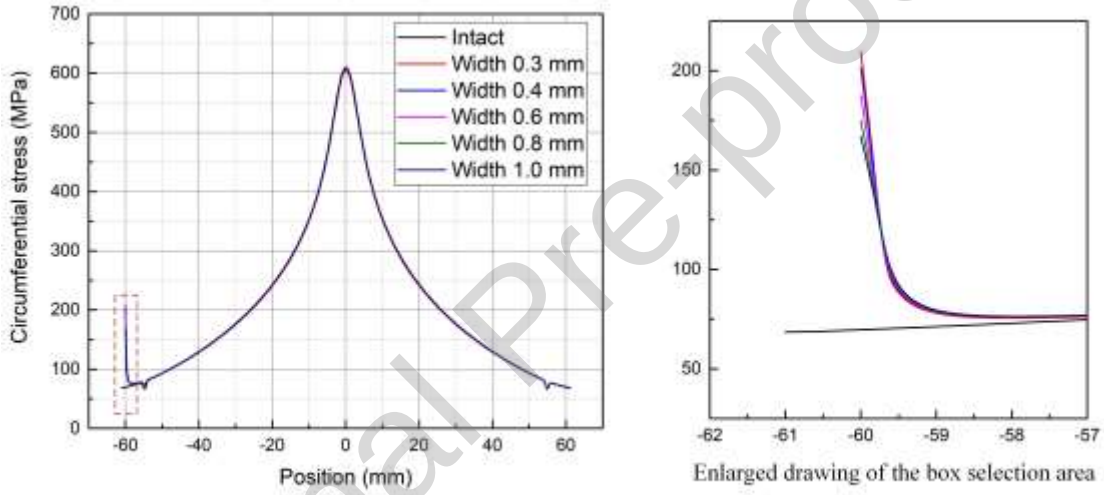

(a) BOR loading on specimens with edge notches of different widths

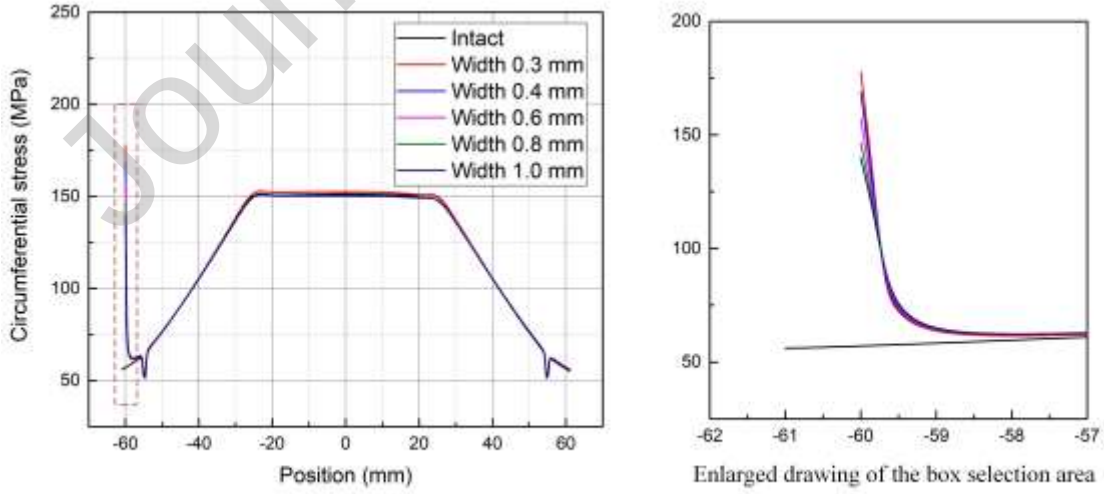

(b) ROR loading on specimens with edge notches of different widths

Fig. 22. Effect of edge notch width on circumferential stress distribution of glass specimens under BOR and ROR loading conditions. The edge notch depth is fixed at 1.0 mm.

As mentioned above, the disc specimen will break from the edge instead of from the center when the edge stress is higher than central stress. To further evaluate the effect of edge defect on failure modes of glass specimens, the ratio between notch tip circumferential stress and central stress is calculated and shown in Fig. 23. In Fig. 23 (a), the edge notch width is fixed at 0.4 mm. For intact specimen, the notch depth can be regarded as zero. The stress ratio increases with the increase of notch depth. In Fig. 23 (b), the edge notch depth is fixed at 1.0 mm. For intact specimen, the notch width can be regarded as infinity. The stress ratio decreases with the increase of notch width.

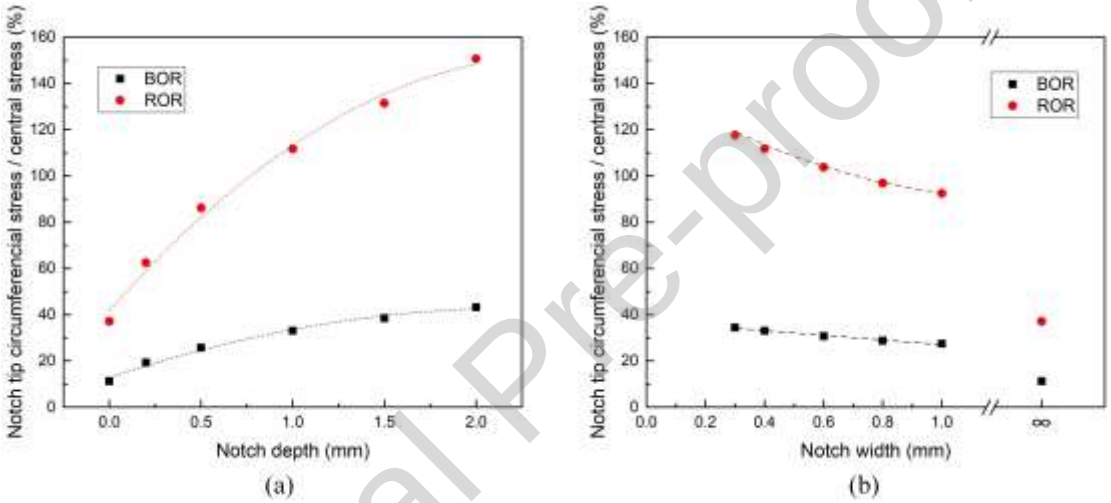

Fig. 23. The ratio of specimen's notch tip circumferential stress and central stress for different (a) notch depth and (b) notch width.

The edge defect of glass plate plays an important role in the biaxial flexural behavior tests and may affect the experimental results, which should be considered and carefully evaluated in related tests. For engineering structures such as windshield of airplanes and glass curtain wall, they are usually installed on the foundation in the form of edge simple support or fixed support. They usually bear biaxial flexural loads during service. The edge defect of glass structures should be examined carefully to avoid crack initiation from the edge section. It should be noted that the geometry of specimens and location of defects will have strong influence on the biaxial flexural response of glass plates. Research on the edge damage of glass plates with complex geometric shapes will be further conducted. Also, it will be worthwhile to incorporate initial surface flaws

or more realistic edge defects into the simulations by developing multiscale models. This would allow for a better understanding of how imperfections interact with the stress field and influence failure mechanisms under biaxial loading.

6. Conclusions

The effect of edge defects and chemical strengthening on the biaxial flexural behavior of aluminosilicate glass plates was investigated in this study. Two loading configurations of biaxial flexural tests, including BOR and ROR, have been conducted on both AG and CSG plates. Edge defects were fabricated on the specimens to further evaluate the influence on biaxial flexural strength and failure mode. The in-plane strain field and out-of-plane displacement field can be obtained based on the 3D-DIC technique and specially designed loading fixture. The BOR flexural strengths of intact AG and CSG specimens are 91.2% and 59.2% higher than their ROR strengths. For comparison of specimens with and without edge defects, there is nearly no difference for AG specimens under BOR loading condition. However, the average BOR flexural strength of CSG specimens with edge defects is 40.4% lower than that of intact specimens. Under ROR loading condition, the flexural strength decreases by 48.3% and 65.1% for AG and CSG specimens when existing edge defects. Radial cracks appear for specimens under BOR loading. Cross cracks appear at the inner ring area with radial cracks outside the inner ring under ROR loading.

Numerical models were built and validated. A gradient stress field is formed on the tensile surface of the disc specimen under BOR loading condition. For ROR loading condition, a uniform equi-biaxially-stressed region is formed in the inner circle region. The different stress distribution forms and randomly distributed surface flaws on glass surface are major causes for different biaxial strength data obtained by different loading configurations. This demonstrates “size effect” of aluminosilicate glass in biaxial flexural tests. The influence of chemically residual stress on the biaxial flexural behavior of aluminosilicate glass plates was also clarified, which can be explained by the coupling effect of residual stress and microscopic surface flaws. The effect of edge defect depth and width on stress concentration has been illustrated. The edge stress

increases with the increase of notch depth and decrease of notch width. These findings can provide technical supports for glass component design and reliability analysis.

Acknowledgements

Supports from National Natural Science Foundation of China (12402447), Beijing Natural Science Foundation (3244028) and R&D Program of Beijing Municipal Education Commission (KM202410005038) are gratefully acknowledged.

References

[1] X. Zhang, Y. Zou, H. Hao, X. Li, G. Ma, K. Liu, Laboratory test on dynamic material properties of annealed float glass, Int. J. Prot. Struct. 3 (2012) 407–430. https://doi.org/10.1260/2041-4196.3.4.407.

[2] B. Jiang, Y. Ding, Y. Guo, Y. Li, Comparative study on the dynamic compressive, tensile and flexural properties of soda-lime silicate glass, Constr. Build. Mater. 388 (2023). https://doi.org/10.1016/j.conbuildmat.2023.131708.

[3] T. Bristogianni, F. Oikonomopoulou, R. Yu, F.A. Veer, R. Nijsse, Investigating the flexural strength of recycled cast glass, Glas. Struct. Eng. 5 (2020) 445–487. https://doi.org/10.1007/s40940-020-00138-2.

[4] Z. Wang, J. Fu, A. Manes, Discrete fracture and size effect of aluminosilicate glass under flexural loading: Monte Carlo simulations and experimental validation, Theor. Appl. Fract. Mech. 111 (2021) 102864. https://doi.org/10.1016/j.tafmec.2020.102864.

[5] A.K. Varshneya, Stronger glass products: Lessons learned and yet to be learned, Int. J. Appl. Glas. Sci. 9 (2018) 140–155. https://doi.org/10.1111/ijag.12341.

[6] G. Macrelli, A.K. Varshneya, J.C. Mauro, Ultra-thin glass as a substrate for flexible photonics, Opt. Mater. (Amst). 106 (2020). https://doi.org/10.1016/j.optmat.2020.109994.

[7] A. Gamal Abd-Elsatar, H. Elsayed, H. Kanková, B. Hruška, J. Kraxner, E. Bernardo, D. Galusek, Ion-exchange enhancement of borosilicate glass vials for pharmaceutical packaging, Open Ceram. 20 (2024).

https://doi.org/10.1016/j.oceram.2024.100689.

[8] Z. Wang, Y. Li, D. Ma, X. Wang, Y. Li, T. Suo, A. Manes, Experimental and numerical investigation on the ballistic performance of aluminosilicate glass with different nosed projectiles, Ceram. Int. 49 (2023) 17729–17745. https://doi.org/10.1016/j.ceramint.2023.02.139.

[9] A.K. Varshneya, Chemical Strengthening of Glass: Lessons Learned and Yet To Be Learned, Int. J. Appl. Glas. Sci. 1 (2010) 131–142. https://doi.org/10.1111/j.2041-1294.2010.00010.x.

[10] B. Egboiyi, R. Mattey, S. Konica, P. Nikam, S. Ghosh, T. Sain, Mechanistic understanding of the fracture toughening in chemically strengthened glass—experiments and phase-field fracture modeling, Int. J. Solids Struct. 238 (2022). https://doi.org/10.1016/j.ijsolstr.2021.111374.

[11] P.P. Hontarovsky, N.V. Smetankina, S.V. Ugrimov, N.H. Harmash, I.I. Melezhyk, Simulation of the Crack Resistance of Ion-Exchange Strengthened Silicate Glass Subject to Bending Strain, Int. Appl. Mech. 58 (2022) 715–724. https://doi.org/10.1007/s10778-023-01195-0.

[12] G. Macrelli, N. Özben, A.C. Kayaalp, M. Çelikbilek Ersundu, İ. Sökmen, Stress in ion exchanged soda-lime silicate and sodium aluminosilicate glasses: Experimental and theoretical comparison, Int. J. Appl. Glas. Sci. 11 (2020) 730–742. https://doi.org/10.1111/ijag.15787.

[13] G. Macrelli, Chemically strengthened glass by ion exchange: Strength evaluation, Int. J. Appl. Glas. Sci. 9 (2018) 156–166. https://doi.org/10.1111/ijag.12291.

[14] Z. Wang, T. Suo, M.Z. Sheikh, Y. Li, X. Wang, Y. Wang, Quasi-static and dynamic flexural behavior of annealed and chemically strengthened aluminosilicate glass with notch defects, J. Non. Cryst. Solids 521 (2019) 119479. https://doi.org/10.1016/j.jnoncrysol.2019.119479.

[15] M.A. Raza, Z. Wang, P. Pei, M. Atif, M.Z. Sheikh, Y. Li, S. Tao, Rate dependent flexural behavior of Aluminosilicate glass: An in-plane and out-of-plane synchronous damage propagation, J. Non. Cryst. Solids 591 (2022). https://doi.org/10.1016/j.jnoncrysol.2022.121747.

[16] L. Ma, M. Mollaali, R. Dugnani, Phase-field simulation of fractographic features formation in soda–lime glass beams fractured in bending, Theor. Appl. Fract. Mech. 127 (2023). https://doi.org/10.1016/j.tafmec.2023.103997.

[17] L. Ma, R. Dugnani, Flexural strength estimation in edge-damaged silicate glass plates by combined phase-field and visual analysis, J. Eur. Ceram. Soc. 44 (2024) 1806–1813. https://doi.org/10.1016/j.jeurceramsoc.2023.10.061.

[18] K. Osnes, T. Børvik, O.S. Hopperstad, Testing and modelling of annealed float glass under quasi-static and dynamic loading, Eng. Fract. Mech. 201 (2018) 107–129. https://doi.org/10.1016/j.engfracmech.2018.05.031.

[19] I. Mohagheghian, Y. Wang, J. Zhou, L. Yu, X. Guo, Y. Yan, M.N. Charalambides, J.P. Dear, Deformation and damage mechanisms of laminated glass windows subjected to high velocity soft impact, Int. J. Solids Struct. 109 (2017) 46–62. https://doi.org/10.1016/j.ijsolstr.2017.01.006.

[20] X. Wu, L. Li, Z. Ding, P. Ji, A Weibull model for bending failure prediction of polyurea laminated glass under coaxial double-ring test, Eng. Fract. Mech. 299 (2024). https://doi.org/10.1016/j.engfracmech.2024.109980.

[21] H.-S. Kim, B.-Y. Yoo, B.-K. Ha, H.-S. Jeong, S.-H. Park, Investigation of stress fields for non-standard sized glass plates loaded by ring-on-ring, J. Eur. Ceram. Soc. 42 (2022) 2429–2440. https://doi.org/10.1016/j.jeurceramsoc.2022.01.015.

[22] K.R. Tekseth, J. Rudshaug, M.G. Mayani, M.N. Akram, T. Børvik, D.W. Breiby, Mapping surface flaws on float glass through Fourier ptychographic quantitative phase imaging, Appl. Phys. Lett. 123 (2023). https://doi.org/10.1063/5.0153216.

[23] A.A. Wereszczak, M.K. Ferber, W. Musselwhite, Method for identifying and mapping flaw size distributions on glass surfaces for predicting mechanical response, Int. J. Appl. Glas. Sci. 5 (2014) 16–21. https://doi.org/10.1111/ijag.12059.

[24] F.A. Veer, Y.M. Rodichev, The structural strength of glass: Hidden damage, Strength Mater. 43 (2011) 302–315. https://doi.org/10.1007/s11223-011-9298-5.

[25] M. Vandebroek, J. Belis, C. Louter, G. Van Tendeloo, Experimental validation of edge strength model for glass with polished and cut edge finishing, Eng. Fract.

Mech. 96 (2012) 480–489. https://doi.org/10.1016/j.engfracmech.2012.08.019.

[26] P. Bukieda, B. Weller, Impact of Cutting Process Parameters on the Mechanical Quality of Processed Glass Edges, in: Challenging Glas. 8 Conf. Archit. Struct. Appl. Glas. CGC 2022, 2022. https://doi.org/10.47982/cgc.8.418.

[27] S. Müller-Braun, M. Seel, M. König, P. Hof, J. Schneider, M. Oechsner, Cut edge of annealed float glass: crack system and possibilities to increase the edge strength by adjusting the cutting process, Glas. Struct. Eng. 5 (2020) 3–25. https://doi.org/10.1007/s40940-019-00108-3.

[28] Z. Wang, T. Guan, T. Ren, H. Wang, T. Suo, Y. Li, T. Iwamoto, X. Wang, Y. Wang, G. Gao, Effect of normal scratch load and HF etching on the mechanical behavior of annealed and chemically strengthened aluminosilicate glass, Ceram. Int. 46 (2020) 4813–4823. https://doi.org/10.1016/j.ceramint.2019.10.214.

[29] J.J. Swab, S.R. Thies, J.C. Wright, J.A. Schoenstein, P.J. Patel, Influence of Surface Scratches on the Flexure Strength of Soda-Lime Silicate and Borosilicate Glass, Exp. Mech. 53 (2013) 91–96. https://doi.org/10.1007/s11340-012-9674-5.

[30] S. Nategh, M. Zaccaria, J. Missinne, J. Belis, Experimental strength characterisation of thin chemically pre-stressed glass based on laser-induced flaws, Glas. Struct. Eng. 7 (2022) 471–486. https://doi.org/10.1007/s40940-022-00205-w.

[31] Z. Pan, J. Yang, X.-E. Wang, C. Zhao, Y. Wang, Y. Zhu, Assessment on flexural performance of monolithic glass considering spatial and depth characteristics of scratches, Eng. Fract. Mech. 300 (2024). https://doi.org/10.1016/j.engfracmech.2024.109964.

[32] Z. Pan, J. Yang, X.-E. Wang, D. Xie, C. Zhao, Scratch-induced micro-fracture behaviour and translational failure of glass: An experimental and numerical study, Thin-Walled Struct. 205 (2024). https://doi.org/10.1016/j.tws.2024.112341.

[33] Y. Xu, S. Liu, L. Ding, J. Li, M. Song, L. Wang, Ion exchange of glass under high pressure, Scr. Mater. 251 (2024).

https://doi.org/10.1016/j.scriptamat.2024.116221.

[34] J. Mao, J. Yuan, Z. Guo, P. Tian, J. Zhang, Q. Zhang, Enhancing bending performance of ultrathin flexible glass through chemical strengthening, Int. J. Appl. Glas. Sci. 15 (2024) 267–275. https://doi.org/10.1111/ijag.16659.

[35] Z. Wang, T. Ren, T. Suo, A. Manes, Quasi-static and low-velocity impact biaxial flexural fracture of aluminosilicate glass — An experimental and numerical study, Thin-Walled Struct. 165 (2021) 107939. https://doi.org/10.1016/j.tws.2021.107939.

[36] G. de With, H.H.M. Wagemans, Ball-on-Ring Test Revisited, J. Am. Ceram. Soc. 72 (1989) 1538–1541. https://doi.org/10.1111/j.1151-2916.1989.tb07702.x.

[37] M.Y. Tsai, T.C. Kuo, A Comparison of Biaxial Bending Strength of Thin Silicon Dies in the Ball-on-Ring and PoEF Tests, J. Electron. Packag. 145 (2023). https://doi.org/10.1115/1.4056717.

[38] D. Deland, Z. Zhang, K. Kirane, Biaxial flexural failure of woven composite plates investigated by the ring on ring bending test, Thin-Walled Struct. 148 (2020). https://doi.org/10.1016/j.tws.2019.106585.

[39] J.J. Swab, P.J. Patel, X. Tran, L. Gilde, E. Luoto, M.H. Gaviola, A. Gott, B. Paulson, S. Kilczewski, Equibiaxial Flexure Strength of Glass: Influence of Glass Plate Size and Equibiaxial Ring Ratio, Int. J. Appl. Glas. Sci. 5 (2014) 384–392. https://doi.org/10.1111/ijag.12094.

[40] EN 1288-2, Glass in Building - Determination of the Bending Strength of Glass - Part 2: Coaxial Double Ring Test on Flat Specimens with Large Test Surface Area, Belgium, 2000.

[41] EN 1288-5, Glass in Building - Determination of the Bending Strength of Glass - Part 5: Coaxial Double Ring Test on Flat Specimens with Small Test Surface Areas, Belgium, 2000.

[42] M.J. Meyland, J.H. Nielsen, C. Kocer, Tensile behaviour of soda-lime-silica glass and the significance of load duration – A literature review, J. Build. Eng. 44 (2021). https://doi.org/10.1016/j.jobe.2021.102966.

[43] W. Shaoshan, L. Xiaogen, R. Meijuan, C. Dake, W. Zhide, Q. Shuang,

Characterization of bending strength of flexible glass under two-point bending, Meas. J. Int. Meas. Confed. 253 (2025). https://doi.org/10.1016/j.measurement.2025.117403.

[44] M.Y. Tsai, H.Y. Liu, Geometric nonlinear effect on biaxial bending strength of thin silicon die in the ball-on-ring test, J. Electron. Packag. 144 (2022). https://doi.org/10.1115/1.4051256.

[45] M.Y. Tsai, T.C. Kuo, P.J. Hsieh, P.S. Huang, Biaxial bending strength of thin silicon dies in the ring-on-ring test by considering geometric nonlinearity and material anisotropy, Mater. Sci. Semicond. Process. 186 (2025). https://doi.org/10.1016/j.mssp.2024.109068.

[46] D. Kinsella, E. Serrano, Failure modelling of glass plates in biaxial loading: using flaw-size based weakest-link systems, Glas. Struct. Eng. 6 (2021) 397–424. https://doi.org/10.1007/s40940-021-00157-7.

[47] Z. Wang, T. Suo, A. Manes, Effect of chemical strengthening residual stress on the flexural performance and fracture behavior of aluminosilicate glass, Eng. Fract. Mech. 258 (2021). https://doi.org/10.1016/j.engfracmech.2021.108104.

[48] S. Hödemann, A. Valdmann, M. Paemurru, J. Anton, V. Kiisk, E. Tkaczyk, J. Kikas, Measurement of stress build-up of ion exchange strengthened lithium aluminosilicate glass, J. Am. Ceram. Soc. 103 (2020) 2407–2420. https://doi.org/10.1111/jace.16913.

[49] N. Terakado, R. Sasaki, Y. Takahashi, T. Fujiwara, S. Orihara, Y. Orihara, A novel method for stress evaluation in chemically strengthened glass based on micro-Raman spectroscopy, Commun. Phys. 3 (2020). https://doi.org/10.1038/s42005-020-0305-7.

[50] X. Nie, W.W. Chen, A.A. Wereszczak, D.W. Templeton, Effect of loading rate and surface conditions on the flexural strength of borosilicate glass, J. Am. Ceram. Soc. 92 (2009) 1287–1295. https://doi.org/10.1111/j.1551-2916.2009.03019.x.

[51] M.J. Meyland, C.K.T. Bønding, R.N.W. Eriksen, J.H. Nielsen, An experimental investigation of the flexural strength of soda–lime–silica glass at high loading

rates, Glas. Struct. Eng. 4 (2019) 175–183. https://doi.org/10.1007/s40940-018-0089-2.

Declaration of interests

☒ The authors declare that they have no known competing financial interests or personal relationships that could have appeared to influence the work reported in this paper.

☐ The authors declare the following financial interests/personal relationships which may be considered as potential competing interests:

Highlights:

- BOR and ROR biaxial flexural behavior was obtained for AG and CSG.
- The strain/stress field and fracture modes of glass plates were analyzed.
- The effect of loading configuration, edge defect and chemical strengthening residual stress were revealed.